1   **Overcoming Resistance to BRAF^{V600E} Inhibition in Melanoma by Deciphering and**

2   **Targeting Personalized Protein Network Alterations**

3   S. Vasudevan[#], E. Flashner-Abramson[#], I. Adesoji Adejumobi, D. Vilencki, S. Stefansky, A.M.

4   Rubinstein and N. Kravchenko-Balasha*

5   Department for Bio-medical Research, Faculty of Dental Medicine, Hebrew University of Jerusalem,

6   Jerusalem 91120, Israel

7   *Corresponding author: natalyk@ekmd.huji.ac.il

8   # Equal contribution

9   **Keywords**

10   Melanoma; information theory; surprisal analysis; patient-specific altered signaling signatures;

11   personalized therapy; BRAF^{V600E}-mutated melanoma

12

13   **Abstract**

14   BRAF^{V600E} melanoma patients, despite initially responding to the clinically prescribed anti-BRAF^{V600E}

15   therapy, often relapse and their tumors develop drug resistance. While it is widely accepted that these

16   tumors are originally driven by the BRAF^{V600E} mutation, they often eventually diverge and become

17   supported by various signaling networks. Therefore, patient-specific altered signaling signatures should be

18   deciphered and treated individually.

19   In this study, we design individualized melanoma combination treatments based on personalized network

20   alterations. Using an information-theoretic approach, we compute high-resolution patient-specific altered

21   signaling signatures. These altered signaling signatures each consist of several co-expressed subnetworks,

22   which should all be targeted to optimally inhibit the entire altered signaling flux. Based on these data, we

23   design smart, personalized drug combinations, often consisting of FDA-approved drugs. We validate our

24   approach in vitro and in vivo showing that individualized drug combinations that are rationally based on

25   patient-specific altered signaling signatures are more efficient than the clinically used anti-BRAF^{V600E} or

26    $BRAF^{V600E}$/MEK targeted therapy. Furthermore, these drug combinations are highly selective, as a drug

27   combination efficient for one $BRAF^{V600E}$ tumor is significantly less efficient for another, and vice versa.

28   The approach presented herein can be broadly applicable to aid clinicians to rationally design patient-

29   specific anti-melanoma drug combinations.

30

31   **Introduction**

32   The rates of melanoma have been rapidly increasing [1]. Melanoma is one of the most common cancers in

33   young adults, and the risk for melanoma increases with age [1]. However, alongside the rapid increase in

34   incidence, there has also been rapid clinical advancement over the past decade, with targeted therapy and

35   immunotherapy that have become available to melanoma patients [2].

36   Melanoma is associated with a great burden of somatic genetic alterations [3], with the primary actionable

37   genomic data being an activating mutation in the BRAF gene, $BRAF^{V600E}$, occurring in ~50% of all

38   melanomas [3,4].

39   Nearly a dozen new treatments have been approved by the Food and Drug Administration (FDA) for

40   unresectable or metastatic melanoma harboring the $BRAF^{V600E}$ mutation, among them vemurafenib (a

41    $BRAF^{V600E}$ inhibitor), cobimetinib (a MEK^{MAPK} inhibitor), or a combination of dabrafenib and trametinib

42   (a $BRAF^{V600E}$ inhibitor and a MEK^{MAPK} inhibitor, respectively) [2].

43   While targeted therapy revolutionized melanoma treatment, the high hopes shortly met a disappointment,

44   as it became evident that most patients treated with $BRAF^{V600E}$ inhibitors eventually relapse and their

45   tumors become resistant to the treatment [5–7]. Various combination treatments were suggested to

46   overcome the acquired resistance to $BRAF^{V600E}$ inhibitors [5,6,9,10]. Nevertheless, $BRAF^{V600E}$ and MEK

47   inhibitors remain the only targeted agents approved by the FDA for melanoma.

48   In this study, we design patient-specific targeted treatments for melanoma based on individualized

49   alterations in signaling protein networks, rather than on genomic or protein biomarkers. Attempting to

50   treat patients based on the identification of single biomarkers or signaling pathways may overlook tumor-

2

51   specific molecular alterations that have evolved during the course of disease, and the consequently

52   selected therapeutic regimen may lack long term efficacy resulting from partial targeting of the tumor

53   imbalance. We have shown that different patients may display similar oncogene expression levels, albeit

54   carrying biologically distinct tumors that harbor different sets of unbalanced molecular processes [11].

55   Therefore, we suggest to explore the cancer data space utilizing an information theoretic approach that is

56   based on surprisal analysis [11–13], to unbiasedly identify the altered signaling network structure that has

57   emerged in every single tumor [11,12].

58   Our thermodynamic-like viewpoint grasps that tumors are altered biological entities, which deviate from

59   their steady state due to patient-specific alterations. Those alterations can manifest in various manners

60   that are dependent on environmental or genomic cues (e.g. carcinogens, altered cell-cell communication,

61   mutations, etc.) and give rise to one or more distinct groups of co-expressed onco-proteins in each tumor,

62   named unbalanced processes [11–13]. A patient-specific set of unbalanced processes constitutes a unique

63   signaling signature and provides critical information regarding the elements in this signature that should

64   be targeted. Each tumor can harbor several distinct unbalanced processes, and therefore all of them should

65   be targeted in order to collapse the altered signaling flux in the tumor [11,12]. We have demonstrated that

66   with comprehensive knowledge about the patient-specific altered signaling signature (PaSSS) in hand, we

67   can predict highly efficacious personalized combinations of targeted drugs in breast cancer [12].

68   Herein, we decipher the accurate network structure of co-expressed functional proteins in melanoma

69   tumors, hypothesizing that the PaSSS identified will guide us on how to improve the clinically used

70   BRAF^{V600E}-targeted drug combinations. Our aim was to examine the ability of PaSSS-based drug

71   combinations to reduce the development of drug resistance, which frequently develops following

72   BRAF^{V600E} inhibition in melanoma.

73   To this end, we studied a dataset consisting of 353 BRAF^{V600E} and BRAF^{WT} skin cutaneous melanoma

74   (SKCM) samples, aiming to gain insights into the altered signaling signatures that have emerged in these

75   tumors. A set of 372 thyroid carcinoma (THCA) samples was added to the dataset, as these tumors

3

76   frequently harbor $BRAF^{V600E}$ as well, therefore enabling studying the commonalities and differences

77   between tumor types that frequently acquire the $BRAF^{V600E}$ mutation.

78   We show that 17 distinct unbalanced processes are repetitive among the 725 SKCM and THCA patient-

79   derived cancer tissues. Each tumor is characterized by a specific subset of typically 1-3 unbalanced

80   processes. Interestingly, we demonstrate that the PaSSS does not necessarily correlate with the existence

81   of the $BRAF^{V600E}$, namely different tumors can harbor different signatures while both carrying the

82   mutated BRAF, and vice versa – tumors can harbor the <u>same</u> altered signaling signature regardless of

83   whether they carry $BRAF^{V600E}$ or $BRAF^{WT}$. These data suggest that examination of the BRAF gene alone

84   does not suffice to tailor effective medicine to the patient. SKCM and THCA patients harboring

85     $BRAF^{V600E}$ can respond differently to the same therapeutic regimen, or rather benefit from the same

86   treatment even though their BRAF mutation status differs.

87   We experimentally demonstrate our ability to predict effective personalized therapy by analyzing a cell

88   line dataset and tailoring efficacious personalized combination treatments to two $BRAF^{V600E}$-harboring

89   melanoma cell lines, A375 and G361. The predicted PaSSS-based drug combinations were shown to have

90   an efficacy superior to monotherapies or other drug combinations (such that were not predicted to target

91   the individualized altered signaling signatures, and combinations used in clinics), both *in vitro* and *in*

92   *vivo*. We show that an in depth resolution of individualized signaling signatures allows inhibiting the

93   development of drug resistance and melanoma regrowth, by demonstrating that while A375 and G361

94   melanomas develop drug resistance several weeks following initial administration of the clinically used

95   combination, dabrafenib+trametinib, individualized PaSSS-based drug combinations gain a longer lasting

96   effect and show high selectivity.

97

98   **Methods**

99   ***Datasets.***

4

100   This study utilized a protein expression dataset consisting of 353 skin cutaneous melanoma (SKCM)

101   sample and 372 thyroid carcinoma (THCA) samples. The samples were selected from a large TCPA

102   dataset containing 7694 cancer tissues from various anatomical origins (PANCAN32, level 4 [14]). Each

103   cancer tissue was profiled on a reverse phase protein array (RPPA) for 258 cancer-associated proteins.

104   After filtering out proteins that had NA values for a significant number of patients, 216 proteins remained

105   for further analysis.

106   The dataset for the cancer cell lines was downloaded from the TCPA portal [14]. The data was already

107   published by Li et al. [15]. A part of the original dataset containing 290 cell lines from 16 types of cancers

108   was selected, including breast, melanoma, ovarian, brain, blood, lung, colon, head and neck, kidney, liver,

109   pancreas, bone and different types of sarcomas, stomach-oesophagus, uterus and thyroid cancers. The

110   cell lines in the dataset were profiled for 224 phospho-proteins and total proteins using RPPA.

111   ***Surprisal analysis***

112   Surprisal analysis is a thermodynamic-based information-theoretic approach [16–18]. The analysis is

113   based on the premise that biological systems reach a balanced state when the system is free of constraints

114   [19–21]. However, when under the influence of environmental and genomic constraints, the system is

115   prevented from reaching the state of minimal free energy, and instead reaches a state which is higher in

116   free energy (in biological systems, which are normally under constant temperature and constant pressure,

117   minimal free energy equals maximal entropy).

118   Surprisal analysis can take as input the expression levels of various macromolecules, e.g. genes,

119   transcripts, or proteins. However, be it environmental or genomic alterations, it is the proteins that

120   constitute the functional output in living systems, therefore we base our analysis on proteomic data. The

121   varying forces, or constraints, that act upon living cells ultimately manifest as alterations in the cellular

122   protein network. Each constraint induces a change in a specific part of the protein network in the cells.

123   The subnetwork that is altered due to the specific constraint is termed an unbalanced process. System can

124   be influenced by several constraints thus leading to the emergence of several unbalanced processes. When

5

125   tumor systems are characterized, the specific set of unbalanced processes is what constitutes the tumor-

126   specific signaling signature.

127   Surprisal analysis discovers the complete set of constraints operating on the system in any given tumor, k,

128   by utilizing the following equation [22]: $\ln X_i(k) = \ln X_i^0(k) - \Sigma G_{i\alpha}\lambda_\alpha(k)$, where i is the protein of interest,

129   X_i^0 is the expected expression level of the protein when the system is at the steady state and free of

130   constraints, and $\Sigma G_{i\alpha}\lambda_\alpha(k)$ represents the sum of deviations in expression level of the protein i due to the

131   various constraints, or unbalanced processes, that exist in the tumor k.

132   The term $G_{i\alpha}$ denotes the degree of participation of the protein i in the unbalanced process α, and its sign

133   indicates the correlation or anti-correlation between proteins in the same process (**Table S1**). Proteins

134   with significant $G_{i\alpha}$ values are grouped into unbalanced processes (**Fig. S1, Table S2**) that are active in

135   the dataset [12].

136   The term $\lambda_\alpha(k)$ represents the importance of the unbalanced process α in the tumor k (**Table S1**).

137   The partial deviations in expression level of the protein i due to the different constraints sum up to the

138   total change in expression level (relative to the balance state level), $\Sigma G_{i\alpha}\lambda_\alpha(k)$.

139   For complete details regarding the analysis please refer to the SI of reference 12.

140   ***Determination of the number of significant unbalanced processes.***

141   The analysis of the 725 patients provided a 725x216 matrix of $\lambda_\alpha(k)$ values, such that every row in the

142   matrix contained 216 values of $\lambda_\alpha(k)$ for 725 patients, and each row corresponded to an unbalanced

143   process (**Table S1**). However, not all unbalanced processes are significant. Our goal is to determine how

144   many unbalanced processes are needed to reconstruct the experimental data, i.e. for which value of n: $\ln$

145    $(X_i(k)/M) \approx -\Sigma G_{i\alpha}\lambda_\alpha(k)$. To find n, we performed the following two steps:

146   (1) **Reproduction of the experimental data by the unbalanced processes was verified**: We plotted

147    $\Sigma G_{i\alpha}\lambda_\alpha(k)$ for $\alpha = 1, 2, ... , n$ against $\ln X_i(k)$ for different proteins, i, and for different values of n, and

148   examined the correlation between them as n was increased. An unbalanced process, $\alpha = n$, was

6

149   considered significant if it improved the correlation significantly relative to $\alpha = n - 1$ (**Fig. S2**)

150   (see [11] for more details).

151   (2) **<u>Processes with significant amplitudes were selected</u>**: To calculate threshold limits for $\lambda_\alpha(k)$ values

152   (presented in **Table S1** and **Fig. S3**) the standard deviations of the levels of the 10 most stable proteins in

153   this dataset were calculated (e.g. those with the smallest standard deviations values). Those fluctuations

154   were considered as baseline fluctuations in the population of the patients which are not influenced by the

155   unbalanced processes. Using standard deviation values of these proteins the threshold limits were

156   calculated as described previously [23]. The analysis revealed that from $\alpha = 18$, the importance values,

157    $\lambda_\alpha(k)$, become insignificant (i.e. do not exceed the noise threshold), suggesting that 17 unbalanced

158   processes are enough to describe the system.

159   For more details see references 12 and 22.

160   *Generation of functional subnetworks.*

161   The functional sub-networks presented in Figures 2, 5, 6, S1 and S4 were generated using a python script

162   as described previously [12]. Briefly, the goal was to generate a functional network according to STRING

163   database, where proteins with negative G values are marked blue and proteins with positive G values are

164   marked red, to easily identify the correlations and anti-correlations between the proteins in the network.

165   The script takes as an input the names of the genes in the network and their G values, obtains the

166   functional connections and their weights from STRING database (string-db.org), and then plots the

167   functional network (using matplotlib library).

168   *Barcode calculation.*

169   The barcodes of unbalanced processes were generated using a python script. For each patient, $\lambda_\alpha(k)$ ($\alpha = 1$,

170   2, 3, …, 17) values were normalized as follows: If $\lambda_\alpha(k) > 2$ (and is therefore significant according to

171   calculation of threshold values) then is was normalized to 1; if $\lambda_\alpha(k) < -2$ (significant according to

172   threshold values as well) then it was normalized to -1; and if $-2 < \lambda_\alpha(k) < 2$ then it was normalized to 0.

7

173   *Cell Culture.*

174   The BRAF mutated melanoma cell lines, A375 and G361, were obtained from the ATCC and grown in

175   DMEM (G361) or RPMI (A375) medium. The cells were supplemented with 10 % fetal calf serum

176   (FCS), L-glutamine (2mM), 100 U/ml penicillin and 100 mg/ml streptomycin and incubated at 37 $^{\circ}$C in

177   5% CO_2. The cell lines were authenticated at the Biomedical Core Facility of the Technion, Haifa, Israel.

178   *Western blot analysis.*

179   The cells were seeded into 6 well plates (~1.5 x 10^6 cells/well) and grown under complete growth media.

180   A375 cells were treated the next day as indicated for 48 hours in partial starvation medium (RPMI

181   medium with 1.2% FCS). G361 cells were treated in complete growth medium for 24 hours. The dead

182   cells were collected from the medium. The adherent cells were then treated with IGF for 15 minutes. The

183   cells were then lysed using hot sample buffer (10% glycerol, 50 mmol/L Tris-HCl pH 6.8, 2% SDS, and

184   5% 2-mercaptoethanol) and western blot analysis was carried out. The lysates were fractionated by SDS-

185   PAGE and transferred to nitrocellulose membranes using a transfer apparatus according to the

186   manufacturer's protocols (Bio-Rad). Blots were developed with an ECL system according to the

187   manufacturer's protocols (Bio-Rad).

188   *Methylene blue assay.*

189   In a 96 well plate, the cells were seeded and treated as indicated for 72 hours. The cells were fixed with

190   4% paraformaldehyde and then stained with methylene blue. To calculate the number of surviving cells,

191   the color was extracted by adding 0.1M Hydrochloric acid and the absorbance was read at 630 nm.

192   *MTT assay.*

193   Cells were seeded and treated as indicated in a 96 well plate for 72 hours. Cell viability was checked

194   using MTT assay kit (Abcam). Equal volumes of MTT solution and culture media were added to each

195   well and incubated for 3 hours at 37 $^{\circ}$C. MTT solvent was added to each well, and then the plate was

8

196   covered in aluminum foil and put on the orbital shaker for 15 minutes. Absorbance was read at 590nm

197   following 1 hour.

198   *Resistance Assay.*

199   Cells were seeded in multiple 96 well plates and treated as needed in various time points (3, 7, 14, 21, 28,

200   35, 42, 49, 54 days). At every time point the cells were fixed with 4% paraformaldehyde and then stained

201   with methylene blue. The number of cells which survived at each time point was quantified by adding

202   0.1M Hydrochloric acid and reading the absorbance at 630 nm.

203

204   *Animal Studies.*

205   The cells - A375 (0.25×10^6 cells/mouse) or G361 (0.5×10^6 cells/ mouse) - were inoculated

206   subcutaneously into NSG mice (n = 8 mice per group), and once the volume of the tumors reached 50

207   mm^3, treatments were initiated 6 times a week for up to 4 weeks. Tumor volume was measured twice a

208   week. Trametinib (0.5mg/kg), dasatinib (35mg/kg) and dabrafenib (35mg/kg) were suspended in an

209   aqueous mixture of 0.5% hydroxypropyl methylcellulose + 0.2% tween 80 and administered by oral

210   gavage. 2-deoxy-D-glucose (500mg/kg) was suspended in saline and injected intraperitoneally. All the

211   drugs were purchased from Cayman chemicals (Enco, Israel). The Hebrew University is an AAALAC

212   International accredited institute. All experiments were conducted with approval from the Hebrew

213   University Animal Care and Use Committee. Ethical accreditation number: Md-17-15174-4.

214
215   **Results**

216   *An overview of the experimental-computational approach*
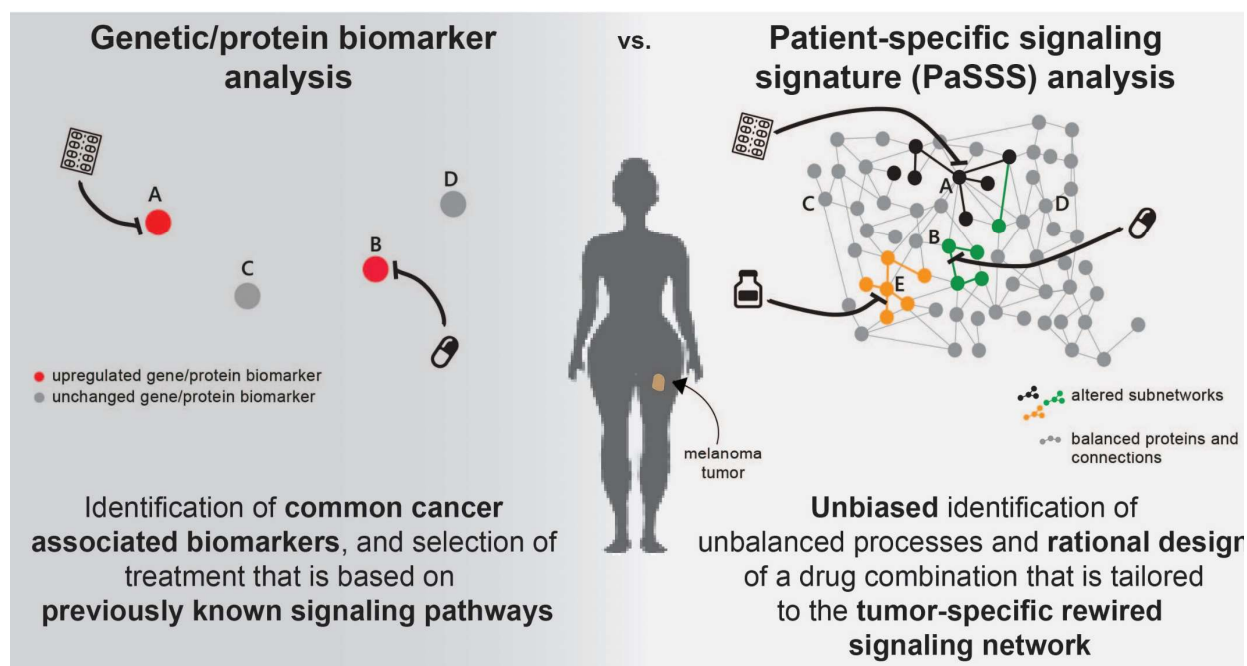
9

Figure 1: Conventional biomarker analysis vs. patient-specific signaling signature analysis. Genetic/protein biomarker analysis relies on evaluation of the expression levels of common cancer type-associated genes or proteins (left). The design of a drug combination is done according to inference of the state of the surrounding signaling network, based on previous knowledge (left). In contrast, patient-specific signaling signature (PaSSS) analysis involves proteomic analysis of hundreds of cancer-associated proteins, and unbiased identification of the altered signaling signature in every sample, i.e. that does not depend on previous knowledge of signaling pathways. This enables rationally designing personalized combinations of targeted drugs that are based on the patient-specific uniquely rewired signaling network (right).

217   Biomarker analysis in melanoma relies mainly on the identification of mutations in the BRAF gene [24].

218   If mutation/upregulation of the mutant BRAF^{V600E} is identified (**Fig. 1**, left), the patient will likely be

219   treated with a BRAF^{V600E} inhibitor (e.g. vemurafenib [25] or dabrafenib [26]), possibly concurrently with

220   an inhibitor of MEK^{MAPK} (e.g. trametinib [27]). The combination of BRAF^{V600E} and MEK^{MAPK} inhibitors

221   was shown to be superior to BRAF^{V600E} inhibition alone and to delay or prevent the development of drug

222   resistance [9].

223   However, the biomarker analysis utilized in clinics lacks information about the altered signaling network,

224   and, for example, may overlook additional or alternative protein targets that, if targeted by drugs, may

225   enhance the efficacy of the treatment (**Fig. 1**, left).

226   We utilize an information theoretic approach that is based on surprisal analysis (**Methods**) [11–13] to

227   gain information regarding the patient-specific signaling signature (PaSSS) that has emerged in every

228   individual tumor (**Fig. 1**, right). Based on proteomic analysis of the samples, we identify the set of altered

229   protein-protein co-expressed subnetworks, or *unbalanced signaling processes,* that has arisen as a result

230   of constraints (environmental or genomic) which operate on the tumor, and then design a combination of

231   targeted drugs that is expected to collapse the tumor-specific altered signaling signature (**Fig 1**, right and

232   **Methods**) [11–13].

233   We obtained from the TCPA database [14] a dataset containing 353 skin cutaneous melanoma (SKCM)

234   and 372 thyroid cancer (THCA) samples (725 samples in total). The thyroid cancer samples were added

235   to the dataset for two main reasons: (1) to increase the number of samples in the dataset, thereby

236   increasing the resolution of the analysis; (2) THCA tumors frequently harbor the BRAF^{V600E} mutation,

237   and we were therefore interested in examining the commonalities and differences between the altered

238   signaling signatures that emerged in SKCM and THCA tumors.

17 unbalanced processes repeat themselves throughout 725 SKCM and THCA tumors

240   The analysis of the dataset revealed that the 725 SKCM and THCA tumors can be described by 17

241   unbalanced processes (**Fig. S1**; the amplitudes for each process in each patient and the importance of each

242   protein in the different processes can be found in **Table S1**; the protein composition of each process is

243   presented in **Table S2**), i.e. 17 distinct unbalanced processes suffice to reproduce the experimental data

244   (**Fig. S2** and **Methods**).

245   Unbalanced processes 1 and 2, the two most significant unbalanced processes, which appear in the largest

246   number of tumors, distinguish well between SKCM and THCA tumors, as can be seen by the 2D plots of

247    $\lambda_\alpha(k)$ values (i.e. amplitudes of each process in every tumor; **Fig. 2A,C,E**). Unbalanced process 1 appears

248   almost exclusively in THCA tumors (372 THCA tumors harbor unbalanced process 1, vs. 46 SKCM

249   tumors; **Fig. 2A,E**, **Table S2**), while unbalanced process 2 characterizes almost exclusively SKCM

11

250   tumors (331 SKCM tumors harbor unbalanced process 2, vs. only 4 THCA tumors; **Fig. 2C,E**, **Table S2**).

251   Unbalanced process 1 involves upregulation of proteins that have been previously linked to THCA:

252   LKB1 [28], fibronectin [29,30], Bcl-2 [31], claudin 7 [32] (**Fig. 2B**). Unbalanced process 2 is

253   characterized by the upregulation of proteins that have been implicated in melanoma, such as Stat5α [33],

254   Akt [34], cKit [35], Her3 [36], and ATM [37] (**Fig. 2D**). As can be seen in the graph in Figure 2C,

255   unbalanced process 2 was assigned a positive amplitude in all 331 SKCM tumors in which it appears,

256   while in 4 THCA tumors it was assigned a negative amplitude (see also **Table S2**). This means that the

257   proteins that participate in this unbalanced process deviate to opposite directions in the two types of

258   tumors (importantly, this remark denotes only the partial deviation that occurred in these proteins due to

259   unbalanced process 2; some of these proteins may have undergone additional deviations due to the

260   activity of other unbalanced processes. See **Table S2** and **Methods**). Although this dominant process

261   appears in a significant number of BRAF$^{\text{V600E}}$ SKCM patients (**Fig. 2C**), it does not include

262   pS(445)BRAF and downstream signaling. This finding corresponds to a recent characterization of

263   melanoma tissues [4] and suggests that the signaling signatures of BRAF$^{\text{V600E}}$ tissues may diverge over

264   time and acquire additional signaling routs which are not necessarily related to the original driver

265   mutations, such as BRAF$^{\text{V600E}}$ or its downstream MEK$^{\text{MAPK}}$ signaling.

266   Unbalanced process 2 can also be found in BRAF$^{\text{WT}}$ patients (**Fig. 2C**). See, for example, patient TCGA-

267   XV-AAZV (**Fig. 3**). The signature of this patient did not include additional processes. A total of 181

268   SKCM patients harbor this signaling signature, consisting only of unbalanced process 2: 100 of them

269   harbor BRAF$^{\text{WT}}$ and 81 of them harbor BRAF$^{\text{V600E}}$ (**Fig. 3**). In contrast, no THCA patients harbor this

270   signature (**Fig. 3**). The finding that BRAF$^{\text{WT}}$ and BRAF$^{\text{V600E}}$ SKCM patients can, in some cases, harbor

271   the same altered signature suggests that these patients can also benefit from the same combination of

272   targeted drugs.

273   Although unbalanced processes 1 and 2 distinguish well between SKCM and THCA patients (**Fig.**

274   **2A,C,E**), these processes alone do not suffice to describe the PaSSS of all patients. Our analysis suggests

12

275   that to decipher the altered signaling signature in every patient, 17 unbalanced processes should be

276   considered. Hence, 2D plots may overlook important therapeutic information. When we inspect the

277   patients in the context of a 17-dimensional space, where each dimension represents an unbalanced

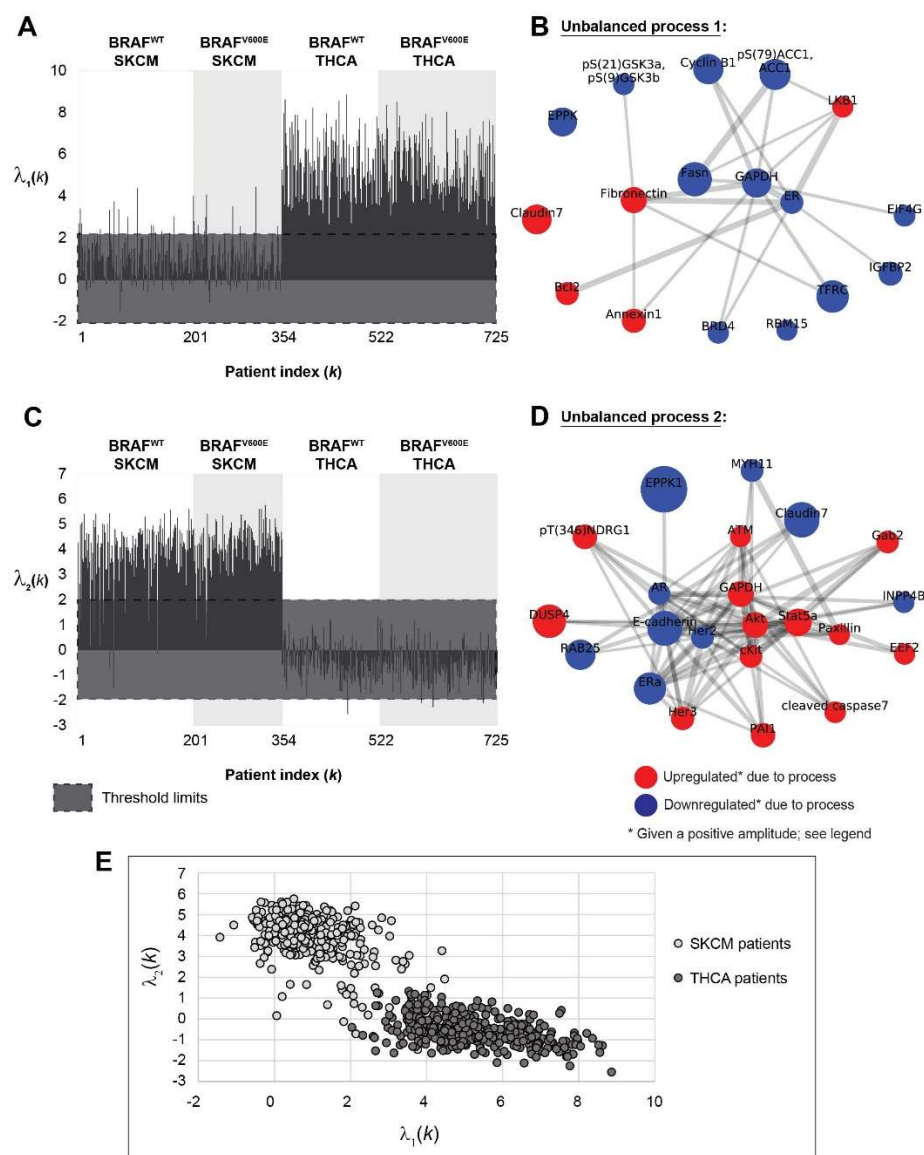278   process, we find that not all SKCM patients harbor unbalanced process 2, and that those who

Figure 2: Unbalanced processes 1 and 2 distinguish well between SKCM and THCA tumors when plotted in 2D. The majority of THCA tumors harbor unbalanced process 1 (**A**), while the majority of SKCM tumors harbor unbalanced process 2 (**C**). Unbalanced processes 1 and 2 are shown in panels **B** and **D**. **Note** that red proteins are upregulated, and blue proteins are downregulated given that the amplitude of the process is positive. In tumors where the amplitude is negative, the direction of change is opposite. (**E**) A 2D plot showing $\lambda_2(k)$ against $\lambda_1(k)$ for all SKCM and THCA patients. The plot shows nicely the separation between SKCM and THCA patients in this 2D space. Note, however, that every tumor is characterized by a set of unbalanced

13

processes (a PaSSS), and that unbalanced processes 1 and 2 alone do not suffice to describe the complete tumor-specific altered signaling signatures.

279   do harbor this process may harbor additional unbalanced processes as well (**Fig. 3** and **Fig. S3**). We have

280   shown that mapping the patients into a multi-dimensional space, a 17D space in our case, allows

281   deciphering the set of unbalanced process, namely the PaSSS, in every tumor. This mapping is crucial for

282   the design of efficacious treatments [12].

283   The SKCM patient TCGA-EB-A5SE, for example, is characterized by a PaSSS consisting of unbalanced

284   processes 2 and 4 (**Fig. 3**). Only 5 SKCM patients were found to be characterized by this set of

285   unbalanced processes. Two of the patients harbor $BRAF^{WT}$ tumors, and 3 of them $BRAF^{V600E}$ (**Fig. 3**).

286   The SKCM patient TCGA-ER-A2NF was found to harbor a PaSSS consisting of unbalanced processes 1,

287   6 and 10 (**Fig. 3**). This patient harbors a one-of-a-kind tumor, as no other patients in the dataset harbor

288   this altered signaling signature (**Fig. 3**).

289   The PaSSS of THCA patient TCGA-DJ-A13V includes unbalanced processes 1 and 4 (**Fig. 3**). This

290   signature characterizes 38 THCA patients, 12 of them $BRAF^{WT}$ and 26 of them $BRAF^{V600E}$ (**Fig. 3**). These

291   THCA patients may benefit from a combination of drugs that target central protein nodes in unbalanced

292   processes 1 and 4, regardless of whether they harbor $BRAF^{V600E}$ or not. No SKCM patients harbor this

293   altered signaling signature (**Fig. 3**).

294   Another interesting finding is that SKCM and THCA patients may harbor the same PaSSS, as is the case

295   of the signature consisting of unbalanced process 1, shared by 3 SKCM patients and 142 THCA patients

296   (**Fig. 3** and **Table S2**). All these patients may be treated with the same drug combination, targeting key

297   proteins in unbalanced process 1, e.g. LKB1 and fibronectin (**Fig. 2B**).

14

Patient index	207	544	242	20	2
Case ID	TCGA-XV-AAZV	TCGA-DJ-A13V	TCGA-EB-A5SE	TCGA-ER-A2NF	TCGA-EB-A5UM
Cancer type	SKCM	THCA	SKCM	SKCM	SKCM
Active unbalanced processes	2^+	$1^+,4^+$	$2^+,4^+$	$1^+,6^+,10^+$	1^+
# of SKCM patients with the same signature (BRAF^{V600E}-/BRAF^{V600E}+)	181 (100/81)	0	5 (2/3)	1 (1/0)	3 (3/0)
# of THCA patients with the same signature (BRAF^{V600E}-/BRAF^{V600E}+)	0	38 (12/26)	0	0	142 (52/90)

298

299 **Figure 3: Examples for patient-specific sets of active unbalanced processes.** Each patient typically harbors a
300 set of 1-3 active unbalanced processes. Our results show that a specific *set* of active processes does not necessarily
301 distinguish between BRAF^{V600E}- and BRAF^{V600E}+ patients, or between SKCM and THCA patients.

302 ***The altered signaling signatures identified in SKCM and THCA are almost mutually exclusive***

303 To explore the entire dataset in terms of the set of unbalanced processes that each patient harbors, we

304 assigned to each patient a patient-specific barcode, denoting the normalized PaSSS, i.e. the active

305 unbalanced processes in the specific tumor, and the signs of their amplitudes (positive/negative)

306 disregarding the size of the amplitude (**Fig. 4, Table S3**). These barcodes represent the mapping of every

307 patient to a 17-dimensional space where each dimension denotes a specific unbalanced process [11,12].

308 We found that 138 distinct barcodes repeated themselves in the dataset (**Table S4**). Interestingly, the

309 barcodes are almost mutually exclusive: 87 of the barcodes characterize SKCM tumors; 84 of them

310 characterize <u>only</u> SKCM tumors and are not harbored by any THCA tumor (**Table S4**). 51 barcodes

311 characterize THCA tumors; of them 48 characterize <u>solely</u> THCA tumors (**Table S4**).

312 Most of the barcodes are rare: 81 barcodes are shared by only 5 SKCM tumors or less; 56 of them
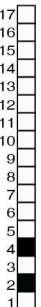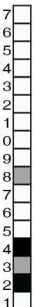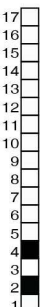
313 describe single, one-of-a-kind SKCM tumors (**Table S4**). 47 barcodes are shared by only 5 THCA tumors

314 or less; 36 of them describe single THCA tumors (**Table S4**). This finding corroborates with our previous

315 studies of signaling signatures in cancer [12], and underscores the need for personalized cancer diagnosis

316 that is not biased by, e.g., the anatomical origin of the tumor.

15

317   *Patient-specific barcodes guide the rational design of personalized targeted combination therapy*

Patient index	238	70	8
Case ID	TCGA-EE-A3AD	TCGA-EE-A180	TCGA-EB-A4XL
Cancer type	SKCM	SKCM	SKCM
BRAF status	BRAF^{V600E}	BRAF^{WT}	BRAF^{WT}
Disease stage	III	III	IIC
Clinical treatment	BRAF^{V600E}+MEK inhibitors	immune checkpoint inhibitors	immune checkpoint inhibitors
SA-identified barcode of unbalanced processes*			
SA-predicted protein targets**	Stat5α, cKit	Stat5α, cKit, Her2/BRAF, pS(473)Akt	Stat5α, cKit

* ■ Active process - positive amplitude ▩ Active process - negative amplitude ☐ Inactive process
** See the full list of process-specific protein targets in Supplementary Table 5

318

319   **Figure 4:** Patient-specific altered signaling signatures, or barcodes, can guide the design of personalized
320   combination therapies. For each tumor, processes with amplitudes exceeding the threshold values (**Methods**) were
321   selected and included in patient-specific sets of unbalanced processes. Those sets were converted into schematic
322   barcodes. Central proteins from each process were suggested as potential targets for personalized drug
323   combinations.

324   We have previously shown the predictive power of our analysis in determining effective patient-tailored

325   combinations of drugs that target key proteins in every unbalanced process [12,13].

326   Utilizing the maps of the unbalanced processes identified in the dataset herein (**Fig. S1**), we predicted

327   process-specific protein targets for each process (**Table S5**). Each individual patient is predicted to

16

328   benefit from a therapy that combines drugs against all the unbalanced processes active in the specific

329   tumor (**Fig. 4, Table S5**).

330   As mentioned above, SKCM patients can in some cases benefit from the same combination therapy,

331   regardless of their BRAF mutational status. This is the case for patients TCGA-EE-A3AD (carrying

332   BRAF^{V600E}) and TCGA-EB-A4XL (carrying BRAF^{WT}), that were found to harbor tumors characterized by

333   the same barcode of unbalanced processes, and were therefore predicted to benefit from the same

334   treatment, where Stat5α and cKit are targeted simultaneously (**Fig. 4**).

335   Patient TCGA-EE-A180 carries BRAF^{WT}, as does patient TCGA-EB-A4XL (**Fig. 4**). However, patient

336   TCGA-EE-A180 harbors two active unbalanced processes that are not active in the tumor of patient

337   TCGA-EB-A4XL – processes 3 and 8 (**Fig. 4**). Therefore, the list of proteins that should be targeted in

338   order to collapse the tumor differs in these patients (**Fig. 4**).

339   ***A375 and G361 melanoma cell lines harbor distinct altered signaling signatures***

340   To experimentally validate our hypothesis that BRAF^{V600E} harboring cells may benefit from drug

341   combinations that are designed based on the PaSSS identified at the time of diagnosis, we turned to

342   analyze a different dataset containing 290 cell lines originating from 16 types of cancer, including blood,

343   bone, breast, colon, skin, uterus, and more (see **Methods**). The cell lines were each profiled for the

344   expression levels of 224 proteins and phosphoproteins using reverse phase protein assay.

345   PaSSS analysis of this cell line dataset revealed that 17 unbalanced processes were repetitive in the 291

346   cell lines (**Table S6, Table S7**, **Fig. S4**).

347   We selected two melanoma cell lines for experimental validation, G361 and A375. Both cell lines harbor

348   the mutated BRAF^{V600E}. In the clinic, patients bearing tumors with BRAF^{V600E} would all be treated

349   similarly, with BRAF inhibitors alone or in combination with MEK inhibitors [9,27].

350   Our analysis, however, shows that G361 and A375 each harbor a distinct PaSSS (**Fig. 5,6**). G361 was

351   found to harbor a PaSSS consisting of unbalanced processes 1 and 6 (**Fig. 5A**). The PaSSS of A375, on

17

352   the other hand, consisted of three unbalanced processes, 1, 3 and 6 (**Fig. 6A**). The full lists of proteins

353   participating in these processes are presented in Table S7, and images of the complete unbalanced

354   processes can be found in Figure S4.

355   To predict cell line-specific drug combinations, central protein targets were selected from each active

356   unbalanced process. In unbalanced process 6, pMEK1/2, GAPDH and PKM2 represent central

357   upregulated proteins (**Fig. 5B, Fig. 6B**). Unbalanced process 3 was characterized by an upregulation of

358   PDGFRβ (**Fig. 6B**), and unbalanced process 1 involved an upregulation of pS6 (**Fig. 5B, Fig. 6B**). We

359   hypothesized that targeting these central proteins will reduce the signaling imbalance in A375 and G361

360   cell lines. Therefore, we predicted that G361 cells will be effectively treated by a drug combination

361   containing trametinib (a pMEK1/2 inhibitor, commonly used for melanoma in clinics; also inhibits pS6

362   [38,39]) and 2-deoxy-D-glucose (2-DG; a glycolysis inhibitor, therefore affecting GAPDH and PKM2

363   levels; **Fig. 5B**). Based on the PaSSS of G361, trametinib should effectively target both unbalanced

364   processes, 1 and 6 (**Fig. 5B**). However, since unbalanced process 6 was assigned a relatively high

365   amplitude in G361 cells (**Table S6**), we predicted that a combination treatment combining trametinib with

366   2DG, which targets additional nodes in unbalanced process 6 (**Fig. 5B**), will more effectively target the

367   PaSSS in G361 cells.

368   For A375, the amplitude of unbalanced process 6 was ~2-fold lower than in G361 cells, and therefore we

369   assumed that trametinib alone should suffice to efficiently reduce the signaling flux through this process.

370   Thus, we predicted that a combination of trametinib and dasatinib (a multi-kinase inhibitor targeting also

371   PDGFRβ) should effectively target the 3 unbalanced processes that constitute the PaSSS of these cells
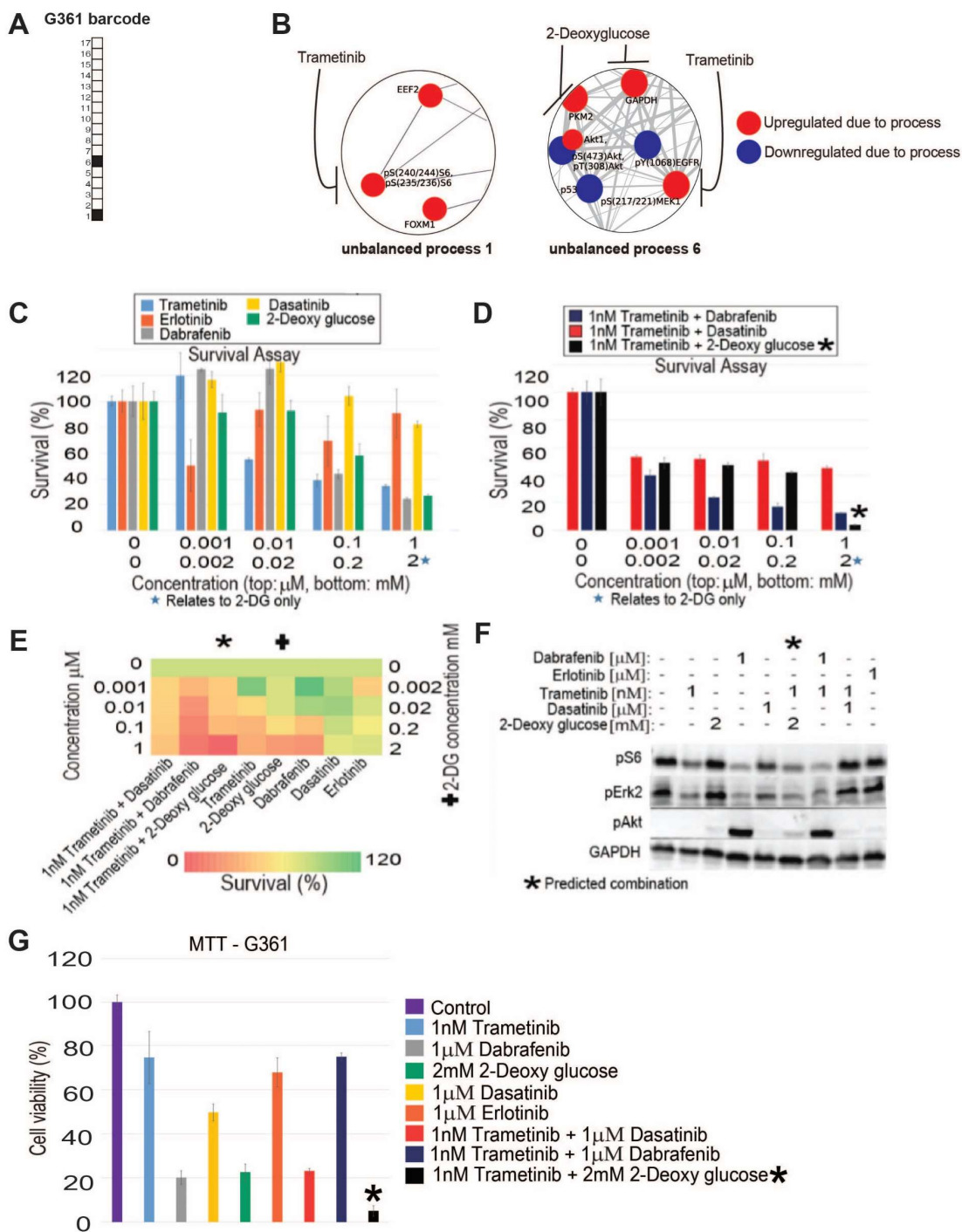
372   (**Fig. 6B**).

18

Figure 5: G361 melanoma cells altered signaling signature and treatment. (**A**) Barcode of active unbalanced processes for G361 based on PaSSS analysis. (**B**) Zoom in images of the active unbalanced processes, 1 and 6, in G361 cells, as well as the drugs targeting the central proteins in each unbalanced process. The upregulated proteins are colored red and the down regulated proteins are colored blue. (**C**, **D**) Survival rates of cells in response to different therapies. The cells were treated with the predicted combination (*) to target G361, the treatments used in the clinics for BRAF mutated melanoma malignancies, monotherapies of each treatment and the predicted combination used to target BRAF mutated melanoma cell

line A375. The combination predicted to target G361 was more efficient than any other treatment. (**E**) Results of the survival assay (shown in panels A and B) are shown as a heatmap. (**F**) Western blot results after treatment with different therapies. The predicted combination depletes the signaling in G361 cells as represented by decrease in phosphorylation levels of pS6, pERK and pAkt. Akt remains active when the cells are treated with dabrafenib or dabrafenib + trametinib. (**G**) G361 cells were treated as indicated for 72 hours and then the viability of the cells was measured in an MTT assay. The effect of the predicted combination (marked in the with an asterix sign) was superior to combinations and single drugs expected to partially inhibit the cell line-specific altered signaling signature.

The predicted drug combinations are cell line-specific and highly efficacious

373

374 Trametinib and dabrafenib, two clinically used drugs, indeed demonstrated relatively efficient killing of

375 G361 cells, achieving up to ~55% and ~75% killing, respectively, when administered to the cells as

376 monotherapies in a range of concentrations between 1 nM and 1 µM (**Fig. 5C**). Based on our analysis, we

377 predicted that these drugs would each partially target the PaSSS in G361 cells (**Fig. 5A,B**).

378 Monotherapies of erlotinib and dasatinib were used as negative controls, as both were not expected to

379 target the altered signaling signature of G361 cells (**Fig. 5C,D**). Indeed, both drugs demonstrated a weak

380 effect on G361 cells, reaching up to ~10% and ~20% killing, respectively (**Fig. 5C,E**). 2-DG, which was

381 predicted to target one of the unbalanced processes active in G361 cells, killed up to ~70% of the cells at

382 2 mM (**Fig. 5C,E**).

383 When we tested combinations of drugs, we found that when G361 cells were treated with a combination

384 of trametinib and dabrafenib, the clinically used combined treatment for BRAF^{V600E} melanoma, the

385 combination was superior to each drug administered alone, and reached ~90% killing of the cells when

386 both drugs were administered at 1 µM (**Fig. 5D,E**). The results of our analysis, however, denoted that

387 other major signaling nodes were altered in G361 cells, and that their targeting by drugs may be beneficial

388 in these cells. When we tested the combination of trametinib and 2-DG, predicted by us to more

389 effectively collapse the PaSSS that emerged in G361 cells, we indeed found that the combination

390 abolished the cells almost completely when trametinib and 2-DG were added at 1 µM and 2mM,

391 respectively (**Fig. 5D,E**). The combination of trametinib and 2-DG also effectively turned off the cellular

392 signaling, as represented by the central proteins S6, Akt and ERK, while the other combinations we tested

20

393   failed to do so (**Fig. 5F**). For example, the clinically used combination, dabrafenib+trametinib, induced

394   the activity of pS(473)Akt (**Fig. 5F**), possibly reflecting a response of the cells to incomplete inhibition of

395   the altered signaling flux.

396   In A375 cells, trametinib, dabrafenib and dasatinib killed up to ~80% of the cells, when administered as

397   single drugs (**Fig. 6C,E**). Erlotinib was used as a negative control, as it was predicted not to target any

398   major node in the PaSSS of A375 cells, and indeed killed only up to ~15% of the cells (**Fig. 6C,E**). 2-DG,

399   which was predicted to target one of the three unbalanced processes active in A375 cells (**Fig. 6A,B**),

400   killed up to ~30% of the cells when administered as monotherapy (**Fig. 6C,E**).

401   The clinically used drug combination, trametinib and dabrafenib, was more effective than each drug

402   alone, and killed up to 90% of the cells (**Fig. 6D,E**). However, as in the case of G361 cells, we predicted

403   that the clinically used combination would not be optimal in A375 cells, because another major node,

404   PDGFRβ, should be targeted as well in order to effectively collapse the PaSSS in A375 cells (**Fig. 6A,B**).

405   We therefore predicted that a combination of trametinib and dasatinib would efficiently target the altered

406   signaling flux generated by 3 unbalanced processes in A375 cells (**Fig. 6A,B**). When we tested this

407   combination, we found that it was highly efficacious and killed up to ~95% of the cells (**Fig. 6D,E**).

408   Moreover, trametinib and dasatinib, when combined, diminished S6 and ERK signaling, and lowered the

409   levels of pPDGFRβ (**Fig. 6F**). As we found in the case of G361 cells, the clinically used combination,

410   trametinib and dabrafenib, invoked an upregulation of pS(473)Akt in A375 cells as well (**Fig. 6F**).

411   We tested the effect of combination predicted for G361 cells, trametinib and 2-DG, on A375 cells, and

412   found that it was less effective in inhibiting the intra-cellular signaling (**Fig. 6F**) as well as cell survival

413   than the drug combination predicted for the PaSSS of A375 (**Fig. 6D,E**). We attribute this finding to the

414   fact the combination of trametinib and 2-DG targets only unbalanced processes 1 and 6, while leaving

415   unbalanced process 3 untargeted, and therefore a partial effect is achieved by these drugs in A375 cells
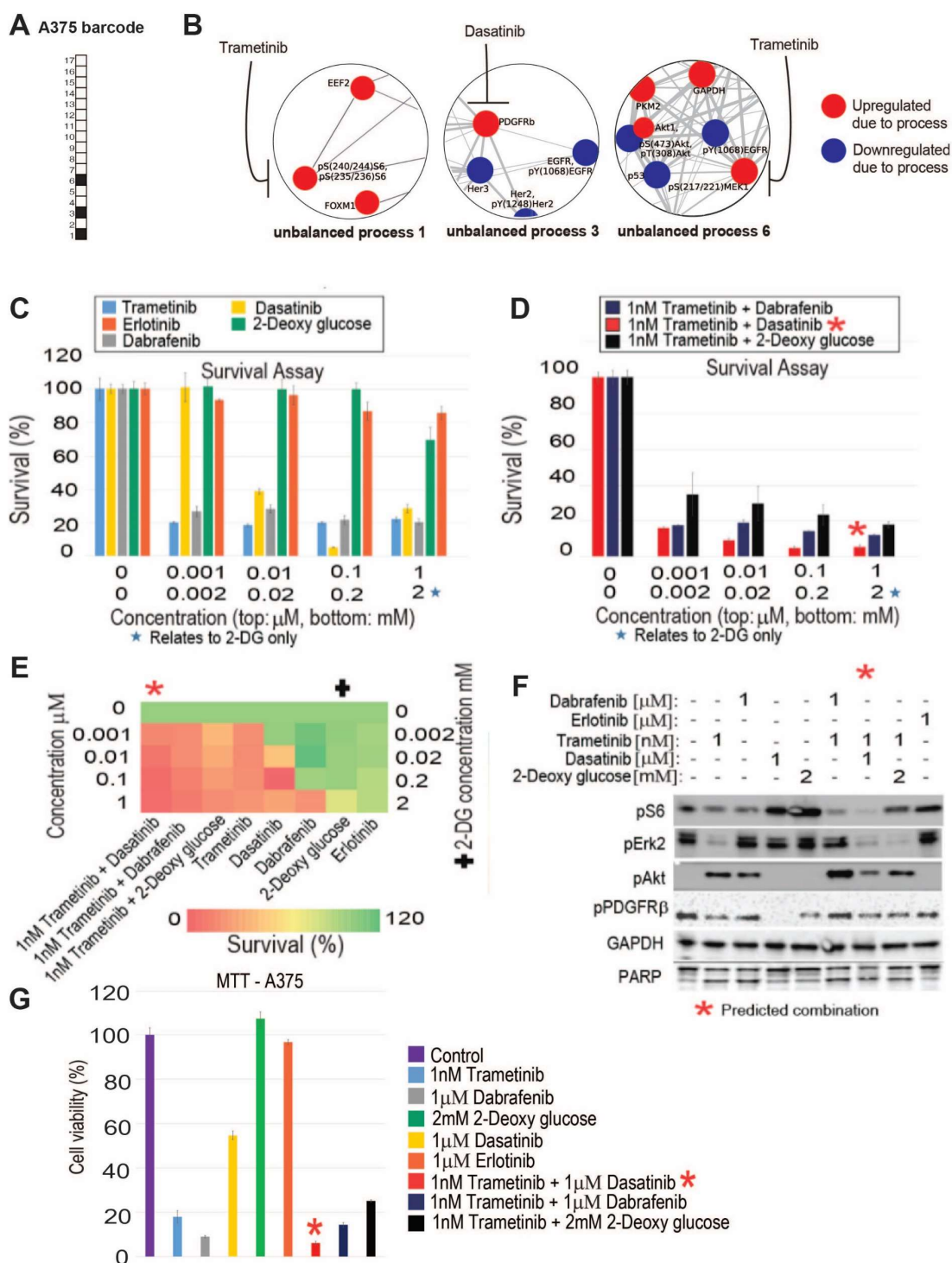
416   (**Fig. 6A,B**).

417

21

Figure 6: A375 melanoma cells altered signaling signature and SA-based treatment. Even though A375 cells harbor BRAF^{V600E}, as do G361 cells, they were found to be characterized by a different set of active unbalanced processes, or PaSSS. (**A**) Barcode of the unbalanced processes for A375 based on PaSSS analysis. (**B**) Zoom in images of the active unbalanced processes, 1, 3 and 6, in A375 cells, as well as the drugs targeting the central proteins in each unbalanced process. The upregulated proteins are colored red and the down regulated proteins are colored blue. (**C**, **D**) Survival rates of cells in response to different therapies.

22

The cells were treated with the predicted combination (*) to target A375, the treatments used in the clinics for BRAF mutated melanoma malignancies, monotherapies of each treatment and the predicted combination used to target BRAF mutated melanoma cell line G361. The combination predicted to target A375 was more efficient than any other treatment. (**E**) Results of the survival assay (shown in panels A and B) are shown as a heatmap. (**F**) Western blot results after treatment with different therapies. The predicted combination depletes the signaling in A375 cells as represented by decrease in phosphorylation levels of pS6, pERK, pAkt and pPDGFRβ. Akt remains active when the cells are treated with monotherapies - trametinib or dabrafenib, and the combination therapies - dabrafenib + trametinib or trametinib + 2-deoxy glucose, the predicted combination of G361. (**G**) A375 cells were treated as indicated for 72 hours and then the viability of the cells was measured in an MTT assay. The effect of the predicted combinations (marked in the figure with asterix signs) was superior to combinations and single drugs expected to partially inhibit the cell line-specific altered signaling signature.

418   When tested in an MTT assay (assessing metabolic activity of the cells), the predicted combinations

419   demonstrated higher efficacy and selectivity and were superior to other drug combinations or to each

420   inhibitor alone (**Fig. 5G, 6G**).

421   ***As opposed to common therapies used in clinics, the rationally designed cell line-specific drug***

422   ***combinations prevented the development of drug resistance***

423   We hypothesized that since our predicted drug combinations target the main altered processes

424   simultaneously, they may delay or prevent the development of drug resistance (**Fig. 7A**). To test this

425   hypothesis, G361 and A375 cells were treated twice a week with single inhibitors or with different

426   combinations of inhibitors, for 4-8 weeks.

427   In G361 cells, 1 nM of trametinib demonstrated little to no effect on the survival of the cells (**Fig. 7B**). 1

428   μM of dabrafenib killed up to ~92% of the cells at day 21, and then the cells began to regrow, even

429   though the drug was still administered to the cells twice a week (**Fig. 7B**). 2 mM of 2-DG killed up to

430   ~78% of the cells at day 7, and then the cells began to regrow regardless of the presence of the drug (**Fig.**

431   **7B**). Combined treatment with trametinib and dabrafenib, a combination expected to partially target the

432   altered signaling signature (**Fig. 5A,B**), effectively killed up to ~96% of the cells at day 21, but then the

433   cells began to regrow at day 28 in the presence of the drugs (**Fig. 7B**). However, when the cells were

434   treated with the G361 PaSSS-based combination, trametinib and 2-DG (**Fig. 5A,B**), the cells continued to

435   die until they reached a plateau at day 21, and no regrowth of the cells was evident (**Fig. 7B**).

23

436 Similar results were obtained in A375 cells: 1 nM trametinib killed 60% of the cells at day 7, and then the

437 effect plateaued until the cells began to regrow at day 56 (**Fig. 7C**). 1 μM dabrafenib killed ~78% of the

438 cells at day 3, and then the cells kept growing till they reached 40% survival on day 56 (**Fig. 7C**). 1 μM

439 dasatinib killed ~40% of the cells at day 3, and then the cells regrew to 100% survival (**Fig. 7C**).

440 Combined treatment with trametinib and dabrafenib achieved 88% killing at day 3, but then the cells grew

441 until they plateaued at ~30% survival at day 56 (**Fig. 7C**). Trametinib and 2-DG killed 55% of the cells at

442 day 3 with an increase in effect over time, reaching a plateau of 15% survival at day 42 (**Fig. 7C**). The

443 A375 PaSSS-based combination, trametinib and dasatinib (**Fig. 6A,B**), demonstrated a significant killing

444 effect that became stronger with time, reaching near complete killing of the cells at 56 days (**Fig. 7C**).

445 These results clearly show that the PaSSS-based combinations predicted for each melanoma cell line

446 prevent cellular regrowth in-vitro. Thus, targeting the actual altered signaling state, identified in the

447 melanoma cells, and not necessarily the primary driver mutations, can be especially effective in disturbing

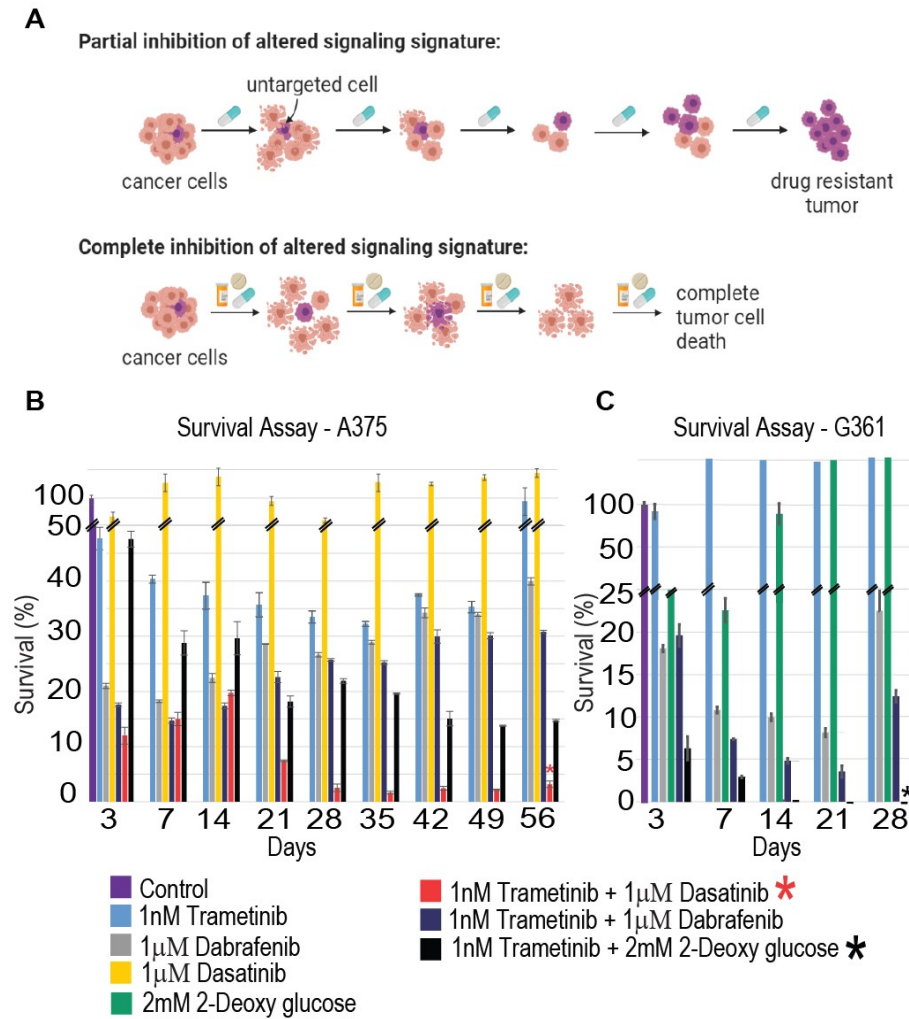448 the signaling flux and preventing cellular regrowth.

Figure 7: Development of resistance to different therapies. (**A**) The development of resistance to different types of therapies is shown in the illustration. The cells were treated with different therapies twice a week and then checked for cell survival. (**B**) A375 cells were treated with the monotherapies, trametinib+dasatinib, dabrafenib+trametinib or trametinib+2-deoxyglucose, twice weekly for 56 days. A development of resistance was evident after 21 days, but not in cells treated with trametinib+dasatinib. (**C**) G361 cells were treated with monotherapies, dabrafenib+trametinib, or trametinib+2-deoxyglucose, twice weekly for 28 days. The cells exhibited signs of drug resistance after 28 days. However, resistance development was not evident in cells that were treated with trametinb+2-deoxyglucose.

449

450 *The predicted drug combinations were superior to clinically used therapies in vivo*

25

451   We turned to examine the effect of the PaSSS-predicted drug combination in murine models. The cells

452   (A375 or G361) were injected subcutaneously into NSG mice, and treatments were initiated 6 times a

453   week for up to 4 weeks (**Fig. 8**).

454   Trametinib alone, or in combination with dasatinib or dabrafenib, was predicted to partially target the

455   PaSSS of G361 cells (**Fig. 5A,B**). And indeed, these treatments demonstrated a reduction in tumor

456   growth, relative to vehicle treatment (**Fig. 8A**). However, the PaSSS-based combination, trametinib + 2-

457   DG, demonstrated the strongest effect, and achieved significant inhibition of G361 tumor growth (**Fig.**

458   **8A**).

459   A375 tumors that were treated with trametinib alone or with a combination trametinib + 2-deoxyglucose

460   (predicted to be efficient for G361 but not for A375 cells (**Fig. 5, 6**)) demonstrated slightly reduced

461   growth relative to vehicle-treated tumors (**Fig. 8B**). When A375 tumors were treated with the clinically

462   used combination, trametinib + dabrafenib, a stronger effect was observed (**Fig. 8B**). PaSSS analysis

463   predicted that trametinib + dabrafenib would achieve partial inhibition of the altered signaling in A375

464   cells (**Fig. 6A,B**), and that adding dasatinib to trametinib should achieve inhibition of intracellular

465   signaling that have emerged in A375 cells (**Fig. 6A,B**). Indeed, the combination trametinib + dasatinib

466   demonstrated an effect superior to all other treatments, and significantly inhibited the growth of A375

467   tumors (**Fig. 8B**).

468   These results point to a significantly higher efficiency of the PaSSS-predicted combinations relative to

469   drug combinations used in clinics. Moreover, we demonstrated the selectivity of the individualized

470   treatments. The predicted and very effective combination for one BRAF^{V600E} melanoma malignancy was

471   significantly less effective for the other, and vice versa (**Fig. 8**). Our results underscore the need for a

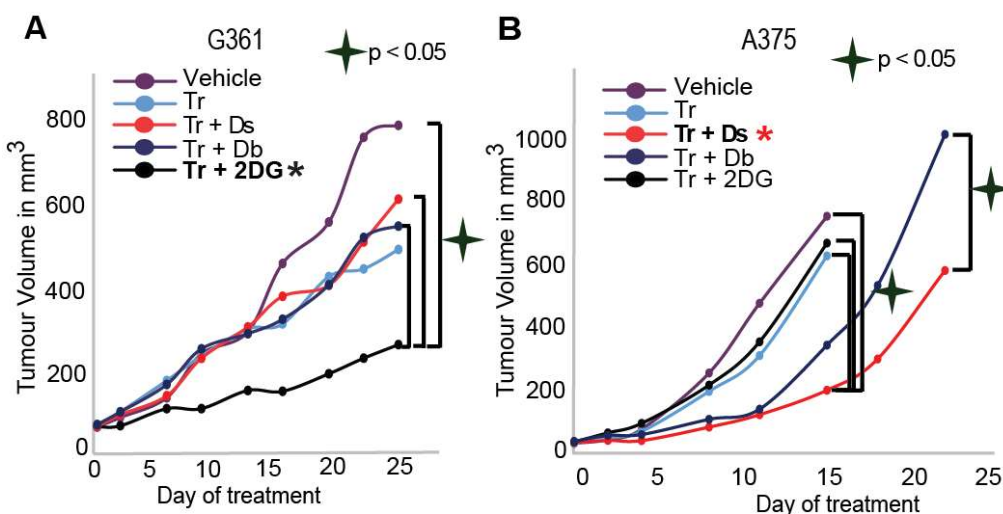472   personalized treatment for each melanoma patient.

26

Figure 8: SA-based drug combinations demonstrated significantly reduced tumor growth *in vivo*. G361 (**A**) or A375 (**B**) were injected subcutaneously into mice, and once tumors reached 50 mm³, treatments were initiated. In both cases, the PaSSS-based drug combinations, predicted to target the cell line-specific altered signaling signature, significantly inhibited tumor growth and demonstrated an effect superior to monotherapy of trametinib or to combinations predicted to partially target the PaSSS (see **Fig. 5,6** for details regarding the altered signaling signatures and PaSSS-based drug combination predictions).

Discussion

With the accelerated gain of knowledge in the field of melanoma therapy and cancer research, it is

becoming clear that tumors evolving from the same anatomical origins cannot necessarily be treated the

same way [40]. Inter tumor heterogeneity results in various response rates of patients to therapy [41–43].

Herein we extend this notion, and show that even tumors that were initially driven by the same

oncogenes, specifically BRAF[V600E]-driven melanoma tumors, often evolve in different molecular manners

[44], giving rise to distinct altered signaling signatures, or PaSSS (patient-specific altered signaling

signature), at the time of biopsy.

We show that 17 altered molecular processes are repetitive among the 725 SKCM and THCA tumors.

Each tumor is characterized by a specific PaSSS, i.e. a subset of ~1-3 unbalanced processes. Accordingly,

each patient is assigned a unique barcode, denoting the normalized PaSSS. We show that the collection of

725 tumors is described by 138 distinct barcodes, suggesting that the cohort of patients consists of 138

types of cancer, rather than only 4 types (SKCM or THCA; BRAF[WT] or BRAF[V600E]). These 138 types of

27

486   tumors, each representing a barcode, or a sub-combination of 17 unbalanced processes, are mapped into a

487   multi-dimensional space, consisting of 17 dimensions. Once the tumor-specific information is

488   transformed into a multi-dimensional space, treating these thousands of tumors becomes at an arm's

489   reach. The specific barcode assigned to each patient allows the rational design of patient-tailored

490   combinations of drugs, many of which already exist in clinics.

491   We found that 353 BRAF^{V600E} and BRAF^{WT} melanoma tumors are described by 87 distinct barcodes of

492   unbalanced processes, and that 372 BRAF^{V600E} and BRAF^{WT} THCA tumors are described by 51 barcodes.

493   Interestingly, the barcodes appeared to be almost mutually exclusive between SKCM and THCA tumors

494   (**Table S4**). While this finding suggests that the molecular processes underlying SKCM and THCA tumor

495   evolution may have organ-specific differences, the large number of cancer type-specific barcodes and the

496   large number of barcodes describing single patients underscore the need for personalized diagnosis and

497   treatment.

498   We show that tumors harboring BRAF^{V600E} can harbor distinct PaSSSs, and in contrast, that tumors can

499   harbor the same PaSSS regardless of whether they carry BRAF^{V600E} or BRAF^{WT}. We therefore deduce

500   that profiling melanoma patients according to their BRAF mutational status is insufficient to assign

501   effective therapy to the patient. Since the unbalanced processes each harbor a specific group of co-

502   expressed altered proteins, they should all be targeted simultaneously to reduce the altered signaling flux

503   in the tumor.

504   We demonstrate this concept experimentally by analyzing a cell line dataset and predicting efficient

505   targeted drug combinations for two selected BRAF^{V600E} melanoma cell lines, G361 and A375. We show

506   that although both cell lines contain the mutated BRAF^{V600E}, they harbor distinct barcodes, and demand

507   different combinations of drugs (**Fig. 5, 6**). We demonstrate that in both cell lines, our PaSSS-based

508   combinations indeed achieved efficient killing of the cells and reached a killing rate that was higher than

509   that of the drug combination often prescribed clinically to BRAF^{V600E} patients, dabrafenib+trametinib .

28

510   These results were recapitulated in vivo as well (**Fig. 8**). Moreover, we demonstrated the selectivity of the

511   PaSSS-based drug combinations. The highly efficient PaSSS-based drug combination for one melanoma

512   malignancy can be significantly less efficient for another melanoma and vice versa.

513   The results reported here highlight the urgent need for the design of personalized treatments for

514   melanoma patients based on individualized alterations in signaling networks rather than on initial

515   mutational events. Furthermore, the study establishes PaSSS analysis as an effective approach for the

516   design of personalized cocktails comprising FDA-approved drugs. Personalized targeted cocktails, which

517   may be further combined with immunotherapy strategies, are expected to provide long term efficacy for

518   melanoma patients.

519

520   **Acknowledgements**

522

523   **Availability of data and materials**

524   The human tumor dataset that supports the findings of this study is publicly available for download from

525   the TCPA portal [14], https://tcpaportal.org/tcpa/download.html > Pan-Can 32.

526   The cell line dataset that supports the findings of this study is publicly available for download from the

527   TCPA portal [14], https://tcpaportal.org/mclp/#/datasets

528

529   **Authors' contributions**

530   N.K.B, S.V. and E.F.A designed the research, N.K.B, E.F.A and S.V carried out computational analyses,

531   E.F.A, S.V, I.A.A, D.V., S.S., and A.A. performed experiments, N.K.B, S.V., and E.F.A wrote the

532   manuscript. All authors approved the manuscript.

533   **Consent for publication**

29

534   The authors confirm that this manuscript does not contain any personal data or images from any

535   individual participants.

536   **Competing interests**

537   The authors declare that they have no competing interests.

538   **References**

539   [1]   NIH. www.cancer.org n.d.

540   [2]   Jenkins RW, Fisher DE. Treatment of Advanced Melanoma in 2020 and Beyond. J Invest

541   Dermatol 2020. https://doi.org/10.1016/J.JID.2020.03.943.

542   [3]   Leonardi GC, Falzone L, Salemi R, Zanghì A, Spandidos DA, McCubrey JA, et al. Cutaneous

543   melanoma: From pathogenesis to therapy (Review). Int J Oncol 2018;52:1071.

544   https://doi.org/10.3892/IJO.2018.4287.

545   [4]   Akbani R, Akdemir KC, Aksoy BA, Albert M, Ally A, Amin SB, et al. Genomic Classification of

546   Cutaneous Melanoma. Cell 2015;161:1681–96. https://doi.org/10.1016/J.CELL.2015.05.044.

547   [5]   C S, L W, S H, GJ H, A P, C R, et al. Reversible and Adaptive Resistance to BRAF(V600E)

548   Inhibition in Melanoma. Nature 2014;508. https://doi.org/10.1038/NATURE13121.

549   [6]   M G, D S, DH J, S M, S C, HJ B, et al. BRAF Inhibitors: Resistance and the Promise of

550   Combination Treatments for Melanoma. Oncotarget 2017;8.

551   https://doi.org/10.18632/ONCOTARGET.19836.

552   [7]   SA L, SA K. Diverse Mechanisms of BRAF Inhibitor Resistance in Melanoma Identified in

553   Clinical and Preclinical Studies. Front Oncol 2019;9. https://doi.org/10.3389/FONC.2019.00268.

554   [8]   Girotti MR, Pedersen M, Sanchez-Laorden B, Viros A, Turajlic S, Niculescu-Duvaz D, et al.

555   Inhibiting EGF receptor or SRC family kinase signaling overcomes BRAF inhibitor resistance in

556   melanoma. Cancer Discov 2013;3:158–67. https://doi.org/10.1158/2159-8290.CD-12-0386.

30

557 [9]   Eroglu Z, Ribas A. Combination therapy with BRAF and MEK inhibitors for melanoma: latest

558   evidence and place in therapy. Ther Adv Med Oncol 2016;8:48–56.

559   https://doi.org/10.1177/1758834015616934.

560 [10] Long G V., Stroyakovskiy D, Gogas H, Levchenko E, de Braud F, Larkin J, et al. Combined

561   BRAF and MEK Inhibition versus BRAF Inhibition Alone in Melanoma. N Engl J Med

562   2014;371:1877–88. https://doi.org/10.1056/NEJMoa1406037.

563 [11] Vasudevan S, Flashner-Abramson E, Remacle F, Levine RD, Kravchenko-Balasha N.

564   Personalized disease signatures through information-theoretic compaction of big cancer data. Proc

565   Natl Acad Sci U S A 2018;115:7694–9. https://doi.org/10.1073/pnas.1804214115.

566 [12] Flashner-Abramson E, Vasudevan S, Adejumobi IA, Sonnenblick A, Kravchenko-Balasha N.

567   Decoding cancer heterogeneity: studying patient-specific signaling signatures towards

568   personalized cancer therapy. Theranostics 2019;9:5149–65. https://doi.org/10.7150/thno.31657.

569 [13] Flashner-Abramson E, Abramson J, White FM, Kravchenko-Balasha N. A thermodynamic-based

570   approach for the resolution and prediction of protein network structures. Chem Phys 2018;514:20–

571   30. https://doi.org/10.1016/j.chemphys.2018.03.005.

572 [14] The Cancer Proteome Atlas Portal n.d. http://tcpaportal.org.

573 [15] Li J, Zhao W, Akbani R, Liu W, Ju Z, Ling S, et al. Characterization of Human Cancer Cell Lines

574   by Reverse-phase Protein Arrays. Cancer Cell 2017;31:225–39.

575   https://doi.org/10.1016/j.ccell.2017.01.005.

576 [16] Levine RD, Bernstein RB. Energy disposal and energy consumption in elementary chemical

577   reactions. Information theoretic approach. Acc Chem Res 1974;7:393–400.

578   https://doi.org/10.1021/ar50084a001.

579 [17] Levine RD. An information theoretical approach to inversion problems. J Phys A Math Gen

580   1980;13:91. https://doi.org/10.1088/0305-4470/13/1/011.

581 [18] Levine RD. Molecular Reaction Dynamics. Cambridge: The University Press; 2005.

31

582   [19]   McMillan WG, Mayer JE. THE STATISTICAL THERMODYNAMICS OF

583   MULTICOMPONENT SYSTEMS. J Chem Phys 1945;13:276–305.

584   https://doi.org/10.1063/1.1724036.

585   [20]   Mayer JE, Mayer MG. Statistical mechanics. 2nd ed. New York: Wiley; 1977.

586   [21]   McQuarrie DA. Statistical Mechanics, 1st ed. Univ Sci Books 2000.

587   http://www.uscibooks.com/mcqstatm.htm (accessed December 10, 2015).

588   [22]   Remacle F, Kravchenko-Balasha N, Levitzki A, Levine RD. Information-theoretic analysis of

589   phenotype changes in early stages of carcinogenesis. Proc Natl Acad Sci U S A 2010;107:10324–

590   9. https://doi.org/10.1073/pnas.1005283107.

591   [23]   Gross A, Levine RD. Surprisal analysis of transcripts expression levels in the presence of noise: a

592   reliable determination of the onset of a tumor phenotype. PLoS One 2013;8:e61554.

593   https://doi.org/10.1371/journal.pone.0061554.

594   [24]   Schadendorf D, van Akkooi ACJ, Berking C, Griewank KG, Gutzmer R, Hauschild A, et al.

595   Melanoma. Lancet 2018;392:971–84. https://doi.org/10.1016/S0140-6736(18)31559-9.

596   [25]   Chapman PB, Hauschild A, Robert C, Haanen JB, Ascierto P, Larkin J, et al. Improved Survival

597   with Vemurafenib in Melanoma with BRAF V600E Mutation. N Engl J Med 2011;364:2507–16.

598   https://doi.org/10.1056/NEJMoa1103782.

599   [26]   Hauschild A, Grob J-J, Demidov L V, Jouary T, Gutzmer R, Millward M, et al. Dabrafenib in

600   BRAF-mutated metastatic melanoma: a multicentre, open-label, phase 3 randomised controlled

601   trial. Lancet (London, England) 2012;380:358–65. https://doi.org/10.1016/S0140-6736(12)60868-

602   X.

603   [27]   Luke JJ, Flaherty KT, Ribas A, Long G V. Targeted agents and immunotherapies: optimizing

604   outcomes in melanoma. Nat Rev Clin Oncol 2017;14:463–82.

605   https://doi.org/10.1038/nrclinonc.2017.43.

606   [28]   Kari S, Vasko V V, Priya S, Kirschner LS. PKA Activates AMPK Through LKB1 Signaling in

32

607   Follicular Thyroid Cancer. Front Endocrinol (Lausanne) 2019;10:769.

608   https://doi.org/10.3389/fendo.2019.00769.

609 [29] Xia S, Wang C, Postma EL, Yang Y, Ni X, Zhan W. Fibronectin 1 promotes migration and

610   invasion of papillary thyroid cancer and predicts papillary thyroid cancer lymph node metastasis.

611   Onco Targets Ther 2017;10:1743–55. https://doi.org/10.2147/OTT.S122009.

612 [30] Sponziello M, Rosignolo F, Celano M, Maggisano V, Pecce V, De Rose RF, et al. Fibronectin-1

613   expression is increased in aggressive thyroid cancer and favors the migration and invasion of

614   cancer cells. Mol Cell Endocrinol 2016;431:123–32. https://doi.org/10.1016/j.mce.2016.05.007.

615 [31] Mitsiades CS, Hayden P, Kotoula V, McMillin DW, McMullan C, Negri J, et al. Bcl-2

616   Overexpression in Thyroid Carcinoma Cells Increases Sensitivity to Bcl-2 Homology 3 Domain

617   Inhibition. J Clin Endocrinol Metab 2007;92:4845–52. https://doi.org/10.1210/jc.2007-0942.

618 [32] Süren D, Yildirim M, Sayiner A, Alikanoğlu AS, Atalay I, Gündüz UR, et al. Expression of

619   claudin 1, 4 and 7 in thyroid neoplasms. Oncol Lett 2017;13:3722–6.

620   https://doi.org/10.3892/ol.2017.5916.

621 [33] Mirmohammadsadegh A, Hassan M, Bardenheuer W, Marini A, Gustrau A, Nambiar S, et al.

622   STAT5 phosphorylation in malignant melanoma is important for survival and is mediated through

623   SRC and JAK1 kinases. J Invest Dermatol 2006;126:2272–80.

624   https://doi.org/10.1038/sj.jid.5700385.

625 [34] Davies MA. The Role of the PI3K-AKT Pathway in Melanoma. Cancer J 2012;18:142–7.

626   https://doi.org/10.1097/PPO.0b013e31824d448c.

627 [35] Carvajal RD, Antonescu CR, Wolchok JD, Chapman PB, Roman R-A, Teitcher J, et al. KIT as a

628   Therapeutic Target in Metastatic Melanoma. JAMA 2011;305:2327.

629   https://doi.org/10.1001/jama.2011.746.

630 [36] Reschke M, Mihic-Probst D, van der Horst EH, Knyazev P, Wild PJ, Hutterer M, et al. HER3 Is a

631   Determinant for Poor Prognosis in Melanoma. Clin Cancer Res 2008;14:5188–97.

33

632   https://doi.org/10.1158/1078-0432.CCR-08-0186.

633   [37] Ivanov VN, Zhou H, Partridge MA, Hei TK. Inhibition of Ataxia Telangiectasia Mutated Kinase

634   Activity Enhances TRAIL-Mediated Apoptosis in Human Melanoma Cells. Cancer Res

635   2009;69:3510–9. https://doi.org/10.1158/0008-5472.CAN-08-3883.

636   [38] Andrikopoulos P, Kieswich J, Pacheco S, Nadarajah L, Harwood SM, O'Riordan CE, et al. The

637   MEK Inhibitor Trametinib Ameliorates Kidney Fibrosis by Suppressing ERK1/2 and mTORC1

638   Signaling. J Am Soc Nephrol 2019;30:33–49. https://doi.org/10.1681/ASN.2018020209.

639   [39] Verduzco D, Kuenzi BM, Kinose F, Sondak VK, Eroglu Z, Rix U, et al. Ceritinib Enhances the

640   Efficacy of Trametinib in BRAF/NRAS-Wild-Type Melanoma Cell Lines. Mol Cancer Ther

641   2018;17:73–83. https://doi.org/10.1158/1535-7163.MCT-17-0196.

642   [40] Robin X, Creixell P, Radetskaya O, Santini CC, Longden J, Linding R. Personalized network-

643   based treatments in oncology. Clin Pharmacol Ther 2013;94:646–50.

644   https://doi.org/10.1038/clpt.2013.171.

645   [41] Fisher R, Pusztai L, Swanton C. Cancer heterogeneity: implications for targeted therapeutics. Br J

646   Cancer 2013;108:479–85. https://doi.org/10.1038/bjc.2012.581.

647   [42] Hinohara K, Polyak K. Intratumoral Heterogeneity: More Than Just Mutations. Trends Cell Biol

648   2019;29:569–79. https://doi.org/10.1016/j.tcb.2019.03.003.

649   [43] Alizadeh AA, Aranda V, Bardelli A, Blanpain C, Bock C, Borowski C, et al. Toward

650   understanding and exploiting tumor heterogeneity. Nat Med 2015;21:846–53.

651   https://doi.org/10.1038/nm.3915.

652   [44] Su Y, Ko ME, Cheng H, Zhu R, Xue M, Wang J, et al. Multi-omic single-cell snapshots reveal

653   multiple independent trajectories to drug tolerance in a melanoma cell line. Nat Commun

654   2020;11:2345. https://doi.org/10.1038/s41467-020-15956-9.

655